Int J Adv Manuf Technol (2015) 79:1095–1108
DOI 10.1007/s00170-014-6532-x

ORIGINAL ARTICLE

Position deviation and springback in V-die bending process with asymmetric dies

Daw-Kwei Leu

Received: 23 April 2014 / Accepted: 20 October 2014 / Published online: 25 February 2015
© Springer-Verlag London 2015

Abstract Novel finite element analyses and a series of experiments are performed to characterize high strength steel sheet metal parts fabricated by asymmetric V-die bending dies. The proposed strategy uses a finite element analysis of elasticity–plasticity to simulate asymmetric V-die bending process and to test its viability for friction contact processes. Accordingly, a series of experiments obtained good agreement with the numerical simulation. The effects of process parameters (*e.g.*, lubrication (contact friction), material properties, and process geometries) on deviation in the bending point were experimentally tested to identify the main parameters of position deviation in sheet metal bending processes. Moreover, effects of springback phenomenon on bending defects and on the precision of an asymmetric bent component are discussed. The results of this study can be considered when developing process design guidelines for asymmetric processes in high strength steel sheets.

Keywords HSS · Deviation · V-die bending · Springforward · Springback

1 Introduction

Sheet metal bending is an essential metalworking process in many industries, particularly the automobile industry. Bending processes are widely used to stamp structural parts such as motor vehicle bumpers. However, since springback and failure can cause major defects during sheet bending, potential improvement in this process has been studied intensively by researchers. For example, Gardiner [1] investigated the springback of metals in the early period. Weinmann and Shippell [2] discussed the effect of tool and workpiece geometries upon bending forces and springback during 90 degree V-die bending of HSLA steel plate. Huang et al. [3] performed an elasticity-plasticity analysis of the V-bending process, and Huang et al. [4] performed an elasto-plastic finite element analysis of V-shape sheet bending. For accurately predicting springback in sheet bending processes, Ogawa et al. [5] developed an elasto-plastic finite element (FE) code and performed validation experiments. In Huang and Chen [6], an incremental elastic–plastic finite element computer code based on an updated Lagrangian formulation was used to simulate successive camber processes of V-die bending of sheet metal. Huang [7] performed an elasto-plastic finite element analysis of a V-die coining process used for bending sheet metal. Thipprakmas [8] performed a finite element analysis of sided coined-bead technique in precision V-bending process. Datsko and Yang [9] reported the correlations between the bendability of materials and their tensile properties in the early period. Takenaka et al. [10] investigated material characteristics associated with bendability and methods for measuring the characteristics. Cupka et al. [11] studied fine bending with counter pressure. Kals and Veenstra [12] investigated the critical radius in sheet bending. Wang et al. [13] developed a mathematical model of plane-strain bending of metal sheet and plate. Leu [14] provided a simplified approach for evaluating bendability and springback in plastic anisotropic sheet metals. Recently, Bakhshi-Jooybari et al. [15] performed experiments and numerical simulations to investigate how significant parameters affect springback in CK67 anisotropic steel sheet under U-die and V-die bending. Narayanasamy and Padmanabhan [16] investigated the application of response surface methodology for predicting bend force during air bending process in interstitial free steel sheet. Their analytical results showed that bend force is mainly

D.-K. Leu (✉)
Department of Mechanical Engineering, Taipei Chengshih University of Science and Technology, No. 2, Xueyuan Road, Beitou, Taipei, Taiwan 112, Republic of China
e-mail: dkleu@tpcu.edu.tw

determined by punch travel followed by punch velocity and punch radius. Farsi and Arezoo [17] developed a new method of adjusting the bending sequence in progressive dies in order to reduce the time and cost of producing complex sheet metal components. Yu [18] studied variation in the elastic modulus during plastic deformation and its effect on springback. Ramezani et al. [19] applied a Stribeck friction model in an FE simulation of springback in high-strength steel sheets during V-bending process. Ramezani and Mohd Ripin [20] modeled dry friction as a function of contact area ratio and strain hardening exponent in a study of V-bending process in aluminum alloy 6061-T4 sheets using ABAQUS/Standard. Kardes Sever et al. [21] investigated how unloading apparent modulus (E-modulus) variation with strain affects springback prediction in V-die bending and U-bending of advanced high strength steel AHSS-DP 780. Fu [22] used ABAQUS FEA software to investigate the effects of springback during air bending of sheet metal. Moreover, Fu and Mo [23] investigated the springback prediction of high-strength sheet metal under air bending and tool design based on GA-BPNN. Some effective methods for predicting and restricting springback have been developed. Malikov et al. [24] performed experiments and analytical calculations to investigate the bending force for air bending of structured sheet metals. Their analytical results showed that bending position and structure location significantly affect bending force. Duc-Toan et al. [25] investigated the prediction of spring-back in V-bending of AZ31 magnesium alloy sheet at various temperatures using material modeling. Although much progress has been made, further theoretical development and experimentation are needed to enable practical applications of these findings.

Because of its high strength and low cost compared to other conventional metals, high strength steel (HSS) is widely used in automotive body structures to reduce weight, which then improves energy efficiency. Herein, asymmetric V-die bending is defined as the use of punch or die radii of unequal size on each side. Figure 1 shows the asymmetric V-die bending model. The practical industrial demands of assembly and multi-forming in precision devices have increased the use of asymmetric bending. However, two common defects in asymmetric bending are (1) an incorrectly positioned bending point in the center part of the punch causing a difference in contact friction force and contact area on both contact sides, *i.e.*, position deviation and (2) a difference in punch or die radii producing a different bend angle after unloading on both sides for the different loading path and contact friction. Until now, the only practical solutions for these problems are those proposed by Leu [26], who investigated the position deviation and springback of V-die bending process with asymmetric bend length.

Moreover, asymmetric V-die bending process is a nonlinear problem of plasticity. Therefore, a precise numerical simulation of the deviation caused by deformation during bending is extremely complex. The complexity results from the high nonlinearity of large deformations such as (1) complex geometric changes caused by large displacements, rotations and strains, (2) nonlinear constitutive behaviors of materials caused by inelastic characteristics of large deformations, and (3) variation in the nonlinear characteristics of deformation-dependent boundary conditions during the loading process. These factors make simulations of the deformation process extremely difficult. The finite element method, which became possible only after sufficient advancement of digital computer technology, is considered an essential tool because of its flexibility and accuracy. It reduces complexity in both geometric and material nonlinear problems, and it effectively models highly nonlinear contact boundary conditions.

Therefore, this study performed finite element analysis and a series of experiments to clarify basic characteristics of HSS sheet during asymmetric V-die bending processes. To enable practical application, a major objective is precisely controlling the position of the bending point and modifying both bent angles identically. The effects of process parameters on position deviation and springback are also considered. The experiments show that all the considered parameters affect position deviation and springback in different ways. The findings of this study can used to establish guidelines for designing tools for stamping of HSS sheets. Accordingly, this study also proposes methods of minimizing these defects in order to obtain a precise asymmetric bent component.

2 Basic analyses

2.1 Variational principle

A modification of the pioneering updated Lagrangian formulation developed by McMeeking and Rice [27] is considered the best formulation for describing the incremental characteristics of plastic flow under deformation. At each time instant, the reference state is updated to coincide with the current deformation state. Therefore, the first order theory is consistent with the accuracy of requirement. By using the Jaumann rate of Cauchy stress, the rate equation for virtual work can be expressed in updated Lagrangian form as follows:

$$\int_V \left(\sigma_{ij}^J - 2\sigma_{ik}\dot{\varepsilon}_{kj}\right)\delta\dot{\varepsilon}_{ij}dV + \int_V \sigma_{jk}L_{ik}\delta L_{ij}dV = \int_{S_f} \dot{f}_i\delta v_i\delta S \quad (1)$$

where $\sigma_{ij}^J\left(=\dot{\sigma}_{ij} - w_{ik}\sigma_{kj} + w_{ik}\sigma_{kj}\right)$ is the Jaumann rate of Cauchy stress $\sigma_{ij}, \dot{\varepsilon}_{ij}$ is the strain rate, $L_{ij}=(\partial v_i/\partial X_j)$ denotes the velocity gradient, X_j is the spatial fixed Cartesian coordinate, v_i is the velocity, $\dot{f}_i$ is the rate of the nominal traction, V is

the material volume, and S_f is the surface on which the traction is prescribed.

2.2 Constitutive model

An FE simulation considers elastic effects caused by elastic loading or plastic unloading. This work assumed the following elasto-plastic constitutive relations:

(i) Elastic behavior: isotropic and linear elasticity with small strain;
(ii) Plastic behavior: rate independent, isotropic strain hardening, von Mises yield function and associative flow rule.

The constitutive relation, which incorporates small elastic-finite plastic deformation behavior, is expressed as

$$\sigma_{ij}^{J} = \frac{E}{1+\nu}\left[\delta_{ik}\delta_{jl} + \frac{\nu}{1-2\nu}\delta_{ij}\delta_{kl} - \frac{3\alpha\left(\frac{E}{1+\nu}\right)\sigma_{ij}^{'}\sigma_{kl}^{'}}{2\overline{\sigma}^{2}\left(\frac{2}{3}H^{'} + \frac{E}{1+\nu}\right)}\right]\dot{\varepsilon}_{kl} \tag{2}$$

where $\sigma_{ij}^{'}$ is the deviatory part of σ_{ij}, H' is the rate of strain hardening, E is the elastic modulus, ν is the Poisson ratio, δ_{ij} is the Kronecker symbol, $\overline{\sigma}$ is equivalent stress governed by the von Mises yield function, and α is the unity for the plastic state and zero for the elastic state or the unloading. All material constants in this simple relation can be determined by a simple tensile test.

The relationship of equivalent stress $\overline{\sigma}$ and equivalent plastic strain $\overline{\varepsilon}_p$ of the material is determined by using the following n-power law to model hardening behavior of deformation:

$$\overline{\sigma} = K\overline{\varepsilon}_p^{n} \tag{3}$$

where n denotes the strain hardening exponent and K is a material constant obtained from a simple tensile test.

2.3 Finite element discretization

As the principle of virtual work rate equation and the constitutive relation are linear equations of rates, they can be replaced by increments defined with respect to any continuously increasing measure, *e.g.*, incrementally increasing tool displacement. All rate quantities can then be replaced by incremental quantities. By performing a standard finite element discretization procedure, Eq. 1 yields a system of algebraic equations, which can be expressed in matrix form as follows:

$$[K]\{\Delta u\} = \{\Delta F\} \tag{4}$$

$$[K] = \sum_{\langle e\rangle}\int_{V<e>}[B]^{T}([D^{ep}]-[Q])[B]dV + \sum_{\langle e\rangle}\int_{V<e>}[E]^{T}[Z][E]dV \tag{5}$$

In these equations, $[K]$ is the global elasto-plastic tangent stiffness matrix, which is considered a constant within each incremental step, $\{\Delta u\}$ denotes the nodal displacement increment, $\{\Delta F\}$ denotes the prescribed nodal force increment, $[D^{ep}]$ is the elemental elasto-plastic constitutive matrix, and $[B]$ and $[E]$ denote the strain matrix and the velocity gradient matrix, respectively. The $[Q]$ and $[Z]$ are the stress correction matrices for each deformation stage.

Under the plane strain condition in this analysis, matrices $[Q]$ and $[Z]$ are explicitly represented as

$$[Q] = \begin{bmatrix} 2\sigma_{xx} & 0 & \sigma_{xy} \\ 0 & 2\sigma_{yy} & \sigma_{xy} \\ \sigma_{xy} & \sigma_{xy} & \frac{1}{2}(\sigma_{xx}+\sigma_{yy}) \end{bmatrix} \quad \text{and} \quad [Z] = \begin{bmatrix} \sigma_{xx} & 0 & \sigma_{xy} & 0 \\ 0 & \sigma_{yy} & 0 & \sigma_{xy} \\ \sigma_{xy} & 0 & \sigma_{yy} & 0 \\ 0 & \sigma_{xy} & 0 & \sigma_{xx} \end{bmatrix} \tag{6}$$

For plastic media, the deformed volume is constant, *i.e.,* incompressible or nearly incompressible. Thus, implementing the fully integrated technique in FE analysis causes excessive constraint in cases of thin plates. This work applied the selective reduced integration (SRI) procedure, which effectively solves volumetrically stiff contribution problems.

2.4 Formulation of friction condition

The friction in the contact zone between workpiece and tool is a key factor in the deformation process. The friction state is described by a modification of the Coulomb friction law proposed by Oden and Pries [28]. Two contact friction states, *e.g.*, sticking and sliding, can be satisfactorily modeled by incremental application of this analytical friction law.

Nodal force $\overrightarrow{F}$ acting on the contact node can be resolved into tangential and normal components f_l and f_n,

$$\overrightarrow{F} = f_l\overrightarrow{l} + f_n\overrightarrow{n} \tag{7}$$

where $\overrightarrow{n}$ is the outward vector normal to the tool surface and $\overrightarrow{l}$ is perpendicular to $\overrightarrow{n}$. Tangential force f_l, which is in the same direction as the sliding direction, is obtained by the friction law

$$f_l = \pm\mu f_n \tanh\left(3\Delta u_l^{rel}/\Delta u_s^{rel}\right) \tag{8}$$

where μ is the friction coefficient, f_n denotes the normal force, $tanh(3\Delta u_l^{rel}/\Delta u_s^{rel})$ is an analytical hyperbolic function used to substitute for a discontinuity in sliding or sticking when applying a friction law such as the Coulomb friction law, Δu_s^{rel} denotes the limit displacement increment for quasi-sticking, and Δu_l^{rel} is the incremental displacement caused by sliding relative to the tool movement. Additionally, $\Delta u_l^{rel}=\Delta u_l-\Delta U\sin\theta$ where θ is the angle between the l-axis and the horizontal axis, Δu_l is the tangential displacement increment of the contact node, and ΔU is the incremental displacement of the tool.

The incremental change in nodal force $\overrightarrow{F}$ acting on the contact node can then be written as

$$\Delta\overrightarrow{F}=\Delta f_l\overrightarrow{l}+f_l\Delta\overrightarrow{l}+\Delta f_n\overrightarrow{n}+f_n\Delta\overrightarrow{n} \tag{9}$$

where Δf_n denotes the increment change in normal force, $\Delta\overrightarrow{n}=\pm\Delta u_l^{rel}\overrightarrow{l}/\rho$, $\Delta\overrightarrow{l}=\mp\Delta u_l^{rel}\overrightarrow{n}/\rho$, and Δf_l denotes the incremental change in tangential force,

$$\Delta f_l=\pm\mu\left[\Delta f_n\tanh\left(\frac{3\Delta u_l^{rel}}{\Delta u_s^{rel}}\right)+\frac{f_n\Delta\left(\Delta u_l^{rel}\right)}{\left(\Delta u_s^{rel}/3\right)\cosh^2\left(3\Delta u_l^{rel}/\Delta u_s^{rel}\right)}\right] \tag{10}$$

where ρ is the tool radius and "±" depends on the tool curvature.

Based on the incremental changes in contact force, the global stiffness matrix with respect to the contact node is

$$\begin{bmatrix} k & \cdots & \cdots \\ \cdots & k_{11}\pm\dfrac{\Delta f_n^{i-1}}{\rho} & k_{12} \\ \cdots & k_{21}\mp\dfrac{\Delta f_l^{i-1}}{\rho} & k_{22} \end{bmatrix}\begin{Bmatrix} \cdots \\ \Delta u_l^i \\ \Delta\bar{u}_n^i \end{Bmatrix} = \begin{Bmatrix} \cdots \\ \pm\dfrac{f_n^{i-1}\Delta U\sin\theta}{\rho}+\Delta f_l^{i-1} \\ \mp\dfrac{f_l^{i-1}\Delta U\sin\theta}{\rho}+\Delta f_n^i \end{Bmatrix} \tag{11}$$

where $\Delta\bar{u}_n$ is a prescribed incremental displacement of the contact node in the normal direction of contact boundary ($\Delta U\cdot\cos\theta$), i denotes the current incremental step, and i-1 denotes the previous incremental step. In the solution scheme, the incremental change in friction force Δf_l on the contact node is calculated iteratively.

The asymmetric stiffness matrix in Eq. 11 is highly complex and requires special consideration. Thus, the incremental terms $\Delta\overrightarrow{n}$ and $\Delta\overrightarrow{l}$ in Eq. 9 and the high-order term Δf_l in Eq. 10 are omitted to simplify the calculation. The incremental tangential force is simplified as

$$\Delta f_l=\pm\mu\Delta f_n\tanh\left(3\Delta u_l^{rel}/\Delta u_s^{rel}\right) \tag{12}$$

The incremental change in nodal force $\overrightarrow{F}$ acting on the contact node is simplified as

$$\Delta\overrightarrow{F}=\Delta f_l\overrightarrow{l}+\Delta f_n\overrightarrow{n} \tag{13}$$

The global stiffness matrix with respect to the contact node can be simplified as follows:

$$\begin{bmatrix} k & \cdots & \cdots \\ \cdots & k_{11} & k_{12} \\ \cdots & k_{21} & k_{22} \end{bmatrix}\begin{Bmatrix} \cdots \\ \Delta u_l^i \\ \Delta\bar{u}_n^i \end{Bmatrix} = \begin{Bmatrix} \cdots \\ \Delta f_l^{i-1} \\ \Delta f_n^i \end{Bmatrix} \tag{14}$$

The proposed solution scheme iteratively calculates the incremental change in friction force on the contact node.

2.5 Weighting factor $r_{\min}$ for the increment of each loading step

Each increment refers to the configuration of the material at the beginning of the increment (updated Lagrangian scheme). The contact condition of the nodes, the separation condition of the nodes, and the state of elements must remain constant during the increment. To meet this requirement and to ensure the accuracy of this explicit integration scheme (static explicit formulation), weighting factor $r_{\min}$ proposed by Yamada et al. [29] is used in the elasto-plastic and contact-separation equations to calculate the size of the increment needed to maintain the linear relation. The size of each loading step is determined by the smallest of the following five r values,

$$r_{\min}=\ \mathrm{MIN}\{r_1,r_2,r_3,r_4,r_5\} \tag{15}$$

- r_1 the equivalent stress of elastic elements that have only reached the current yield surface
- r_2 the limit on the largest equivalent strain increment for a linear relation
- r_3 the limit on the rotation increment for a linear relation

r_4 a free node that only contacts the tools
r_5 a contact node that only departs from the tool surface

The above values are consistent with the first order theory. Further details about weighting factor $r_{\min}$ can be found in [30].

2.6 Unloading process

To determine the final shape or the springback behavior, the unloading process is executed under the assumption that the properties of all elements are elastic. The force of the contact node is reversed so that it becomes the prescribed force boundary condition. All tools are removed for the elastic unloading procedure.

2.7 Summary of solution procedure

The algorithm for modeling the sheet metal bending process is summarized as follows:

(1) Set up the initial conditions, and prescribe the boundary conditions and a fictitious tool displacement increment ΔU at the start of the loading.
(2) Calculate stiffness matrix [K], and solve the stiffness equation for a fictitious solution Δu ($=[K]^{-1}\{\Delta F\}$) correspondent to the previous tool displacement.
(3) Determine weighting factor $r_{\min}$= MIN$\{r_1,r_2,r_3,r_4,r_5\}$ for the current step, $0 < r_{\min} \leq 1$.
(4) A "real" solution $u^i = u^{i-1} + r_{\min} \times \Delta u^i$ that validates each condition is used to update the geometry of the deformed sheet and to update the displacements, stresses, and yield limit of each element and boundary conditions of each contact element.
(5) If the prescribed punch displacement is reached, execute the unloading procedure, and output the total results; otherwise, go to step (2).

2.8 FE simulation of asymmetric V-die bending

Figure 1 shows the asymmetric V-die bending model. Figure 2 shows the dimensions of the simulated tools. The asymmetric bending model is either an A1 type or an A2 type. Table 1 shows that the simulated HSS material is a sheet of JIS G3135 SPFC 440 with length, 45 mm; thickness, t=1.4 mm, which are the same specifications used in [26]. In simulation and experiment, the bottom point of punch is set in the center point of test piece as the initial condition of bending. Based on the contact of the sheet metal surface as described in [30, 31], the simulation assumes a friction coefficient of μ=0.1. A four-node bilinear quadrilateral element with the selective reduced integration, which is efficient for sheet metal forming, is used

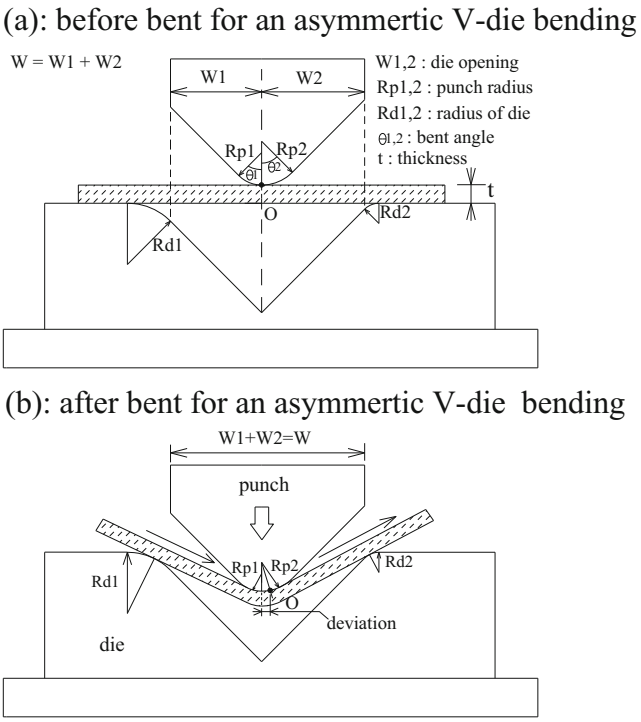

Fig. 1 Scheme of **a** asymmetric bending and **b** position deviation during asymmetric bending

in simulation. Figure 3 shows the simulation results for bending force in the asymmetric V-die bending processes. The distribution of bending force in Fig. 3 shows no difference between the A1 and A2 types. The similar bending forces may result from the similar (but opposite) punch radius dimensions in the A1 and A2 types. Asymmetric and conventional V-die bending processes appear to have a similar distribution of bending force.

Figure 4 shows the simulation results for A1 in all bending processes of asymmetric V-die bending. The black area shows the plastic deformation, and the arrows show the direction of material flow during bending. The area of plastic deformation (black area in Fig. 4a) is symmetrically distributed over the region under the punch during the early stage of bending. However, the plastic deformation area alternates between the right and left sides during the final stages. The extent of bending, however, is clearly greater in the small die radius than in the large die radius. Thus, the small die radius has a larger contact zone, which induces a larger friction force. Accordingly, the higher friction force in the small die radius induces a higher sliding resistance. As bending progresses towards the bottom of the die, a deviation phenomenon occurs, which causes the sheet to move to the side with the small die radius on the punch surface during the final stage. In Fig. 4a, checkpoint O, which was marked on the bottom of punch in the central line (U=0.0 mm) before bending, has obviously moved to the side with the small die radius after bending (U=16.9 mm), which clearly shows the position

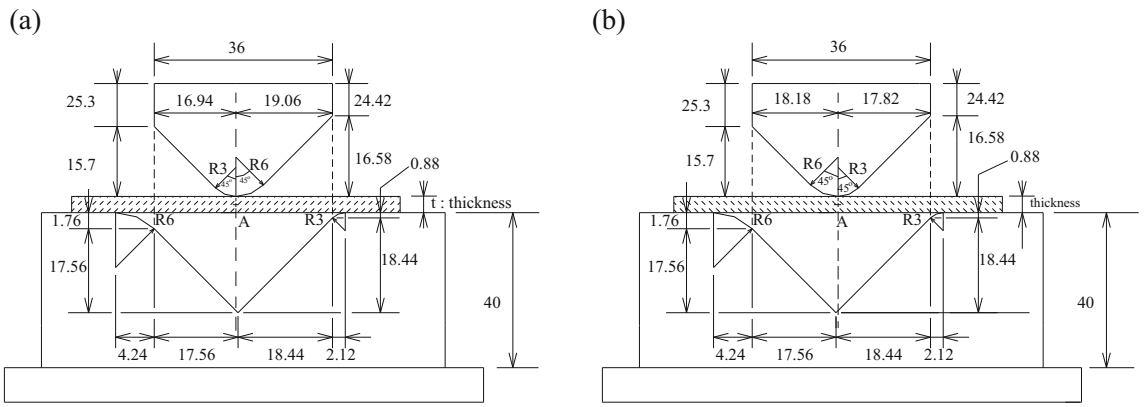

Fig. 2 Schematic representations of asymmetric V-die bending process in **a** A1 and **b** A2 types

deviation phenomenon in asymmetric bending. Here, position deviation e is defined as the horizontal movement of point O.

Accordingly, a springback phenomenon occurs during unloading. In the last line drawing in Fig. 4b, the arrows on both sides of the node, which indicate the direction of incremental displacement of the node, point outward due to elastic recovery during unloading, *i.e.*, the final bent angle is larger than the punch angle. Conversely, the arrows on both sides of the node point inward due to elastic recovery or because the final bent angle is smaller than the punch angle is defined as springforward phenomenon. Deviations in asymmetric bending processes are also apparent in the varying distribution of node displacement. In the bent length of the sheet, the side with the small die radius has a smaller displacement increment in the node compared to the side with the large die radius, which shows that the sliding resistance is greater in the small die radius than in the large die radius. Thus, the different sliding resistance between the small and large die radii causes deviation phenomena during asymmetric V-die bending. In Fig. 4b, the directions of arrows of nodes show a bending rotation on both sides from U=1.0 to 8.0 mm. From U=9.0 to 16.9 mm, the directions of arrows of nodes indicate alternate rotation and sliding phenomena in the contact region on both sides. At U=9–11, 13, and 15 mm, the nodes gradually move from the left side to the right side which has a small die radius as bending proceeds, and the right side simply shows a bending rotation. Conversely, at U=12, 14, and 16.5 mm, the nodes gradually move from the right side to the left side which has a large die radius, and the left simply shows a bending rotation. Both sides show a complex interaction between alternate rotation and movement. Specifically, both sides simultaneously move downward to the central part of punch at U=16 mm. Finally, deviation occurs when the nodes on the left side, which has a larger die radius, move to the right side, which has a small die radius, during the bottom stage. Notably, a change occurs in the last step of U=16.9 mm (the gap between the punch and die equals the sheet thickness), *i.e.*, coining (bottom) effect, so the arrows of the node on both sides point in an outward direction under bending (loading). The observations showed that the variation in the coining (bottom) effect under V-die bending significantly affects elastic recovery.

The simulations in this study confirmed that FE is a powerful tool that accurately depicts processes and variations in deviation during asymmetric bending.

3 Experiment, results, and discussion

The material used in a series of experiments to explore the characteristics of asymmetric bending was HSS SPFC of JIS G3135. The rim of the sheet was polished to remove irregularities and to obtain a smooth surface. Table 1 shows its mechanical properties. Table 2 shows the dimensions of the experimental tools (total eight sets) and the experimental values of deviation and springback angle in the A1 and A2 types shown in Fig. 2. Two lubrication conditions, lubrication

Table 1 Material properties of high strength steel manufactured by China Steel Company

JIS G3135	E/GPa	ν	σ_y/MPa	$\overline{\sigma} = K\overline{\varepsilon}_p{}^n$/MPa	t/mm
SPFC 440	205	0.3	285.9	$\overline{\sigma} = 745.9\overline{\varepsilon}_p{}^{0.212}$	1.4
SPFC 440	205	0.3	313.9	$\overline{\sigma} = 739.9\overline{\varepsilon}_p{}^{0.201}$	1.8
SPFC 590	205	0.3	287.8	$\overline{\sigma} = 1161.6\overline{\varepsilon}_p{}^{0.257}$	1.8

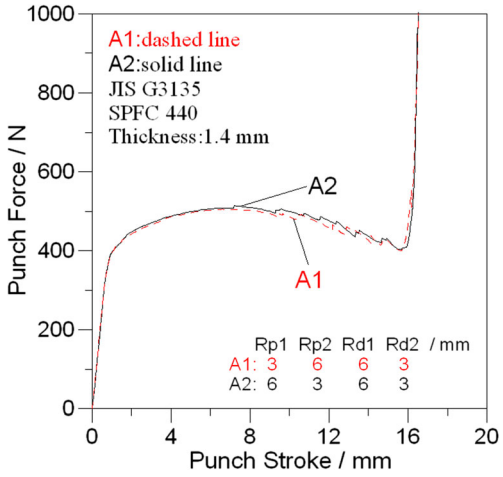

Fig. 3 Relationship of punch force to punch stroke in asymmetric V-die bending: comparison between A1 and A2 types

with WD-40 mineral oil and dry friction (without lubrication), are used in the experiment, and the polished steel sheets used in the experiment are prepared by pressing. The experiments were performed with a 300-kN hydraulic test machine, and optical equipment was used to record the deviation in the bending point. The experimental procedure was as follows: (1) prepare the blanks and record the dimensions of the blanks, the punch head, and the die; (2) set the die assembly onto the hydraulic test machine; (3) apply a thin film of lubricant to the blank and position the blank on the die; (4) set the punch speed to 1 mm/s for the punch head to bend the sheet; and (5) record the deviation in the bending point and springback angle by using optical measuring equipment.

3.1 Verification of the proposed model

Figure 5 shows the simulation results for the eight experimental tools shown in Table 2, including position deviations and springback angles in the final stage. The FE model was then verified by comparing the FE simulation results with the experimental results. Table 2 compares the experimental and calculation results for the eight experimental tools, which shows that the errors, *i.e.*, the difference between calculation and experiment, are acceptable. The deviation errors ranged from 0.35 to −0.12 in all the cases except case 1, in which the error was 0.58; and the errors of springback angle are located at the region from 1.42 to −0.99 except the case 1 which error is 3.8. The larger error of case 1 in Table 2 seems to result from an improper procedure as carrying out the experiment of case 1. Notably, the position deviation was always toward the side with the small die radius. The die radius clearly has an important effect on deviation. Table 2, however, shows fairly good agreement between the calculation results and the experimental results.

3.2 Effects of process parameters on deviation and springback

(1) Position deviation: Figs 6, 7, 8, and 9 show how various process parameters affect position deviation. Figure 6 shows that deviation increases as thickness increases when the parameters are set to Rp1=6 mm, Rp2=3 mm (punch: R6-R3) under Rd1=6 mm, Rd2=3 mm, W=36 mm, dry friction, and SPFC 440. Conversely, deviation decreases as thickness increases when the parameters are set to Rp1=3 mm, Rp2=6 mm (punch: R3–R6) under the same conditions of Rd1, Rd2, W, dry friction, and SPFC 440. This reverse effect may result from the increased friction force on the side with the small punch radius, which causes the bending moment to increase as thickness increases. A complex interaction occurs in which punch radius apparently counteracts the effect of thickness on deviation. Figure 7 shows that the deviation obtained after lubrication with mineral oil WD-40 (small friction effect) is larger than that under dry friction (large friction effect) under Rp1=3 mm, Rp2=6 mm, Rd1=6 mm, Rd2=3 mm, W=36 mm, and t=1.8 mm for both SPFC 440 and 590. Accordingly, the deviation between dry friction and lubrication for SPFC 590 is greater than that for SPFC 440. Clearly, lubrication substantially affects the amount of deviation, and its value, *i.e.*, friction coefficient, is always difficult to be determined. Additionally, the deviation values for SPFC 440 were consistently larger than those for SPFC 590 without the lubrication effect. A high material strength induces a high resistance of movement in the contact region and reduces the position deviation in sliding direction. In cases (ii) and (iii) in Fig. 8, the deviation induced by Rp1=6 mm and Rp2=3 mm is larger than that induced by Rp1=3 mm and Rp2=6 mm when the parameters are set to Rd1=6 mm, Rd2=3 mm, t=1.8 mm, W=36 mm, and dry friction for SPFC 440 and 590. Accordingly, the difference in deviation between (Rp1=6 mm and Rp2=3 mm) and (Rp1=3 mm and Rp2=6 mm) is greater for SPFC 590 than for SPFC 440. These experimental results are consistent with those in Fig. 6. In cases (i) and (iii), the deviation induced by Rp1=6 mm and Rp2=3 mm is smaller than that induced by Rp1=3 mm and Rp2=6 mm when the parameters are set to Rd1=6 mm, Rd2=3 mm, W=36 mm, dry friction and SPFC 440 for t=1.4 mm in case (i). Conversely, the deviation induced by Rp1=6 mm and Rp2=3 mm is larger than induced by Rp1=3 mm and Rp2=6 mm when the parameters are set to t=1.8 mm and under similar Rd1, Rd2, W, dry friction, and SPFC 440 in case (iii). Comparison of cases (i) and (iii) show a complex interaction in which thickness apparently counteracts the effect of punch radius on deviation changes. This reverse effect clearly shows the important effect of thickness on

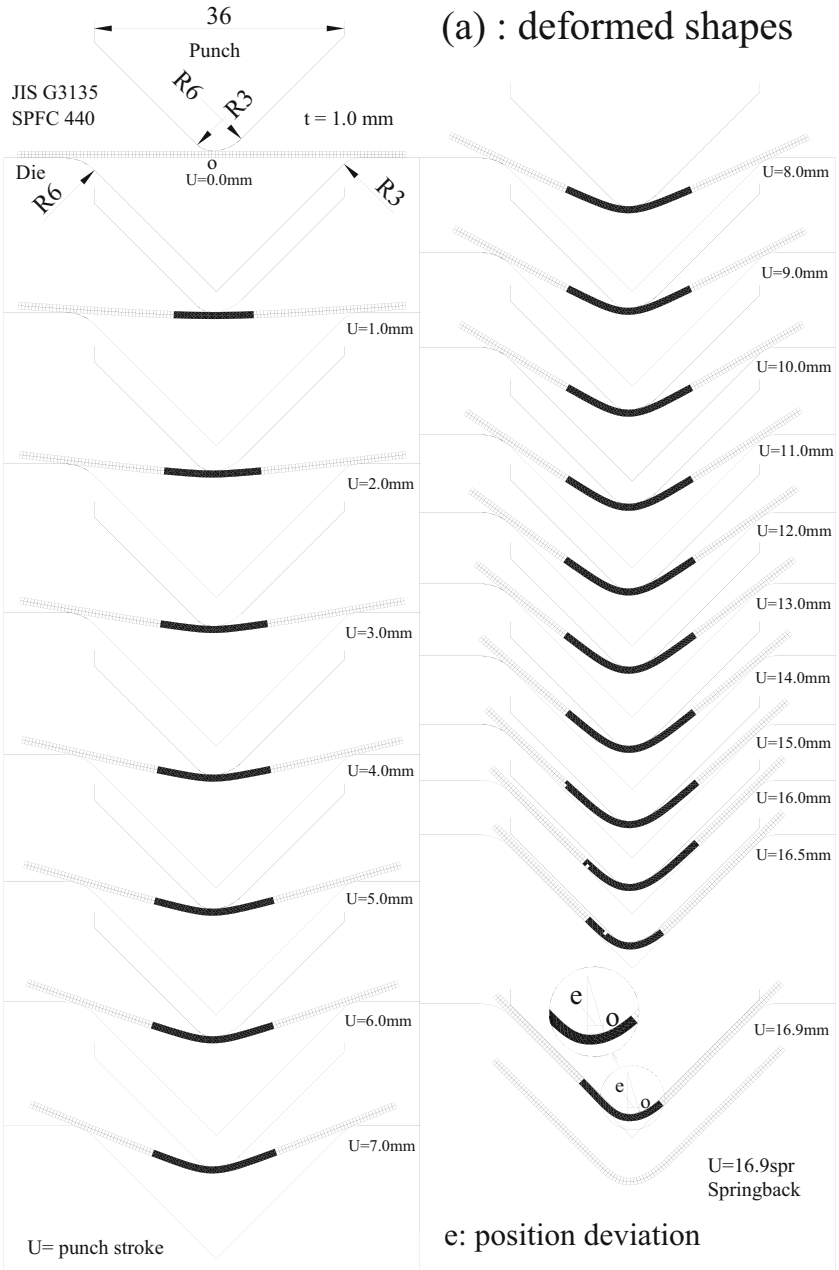

Fig. 4 Simulation of asymmetric bending process in A1 type with μ= 0.05: distributions of **a** deformation processes and **b** displacement increment. The *black area* shows plastic deformation and the arrows show the direction of material flow. *U* is punch stroke. The *last line drawings* of **a** and **b** show the occurrence of springback during unloading

deviation change. The interaction between sheet thickness and punch radius is complex. Cases (ii) and (iii) in Fig. 9 confirm that deviation decreases as material strength increases when the parameters are set to Rp1= 3 mm and Rp2=6 mm, Rd1=6 mm, Rd2=3 mm, t= 1.8 mm, and W=36 mm for lubrication or dry friction. Accordingly, the difference in deviation is greater under dry friction than under lubrication. In cases (i) and (ii), deviation increases as material strength increases under Rp1=6 mm and Rp2=3 mm when the parameters are set to Rd1=6 mm, Rd2=3 mm, W=36 mm, dry friction, and t=1.8 mm in case (i). In case (ii), however, deviation decreases as material strength increases when the parameters are set to Rp1=3 mm and Rp2=6 mm under same Rd1, Rd2, t, and lubrication. Comparison of cases (i) and (ii) shows a complex interaction in which punch radius apparently counteracts the effect of material strength on deviation changes. This reverse effect shows the

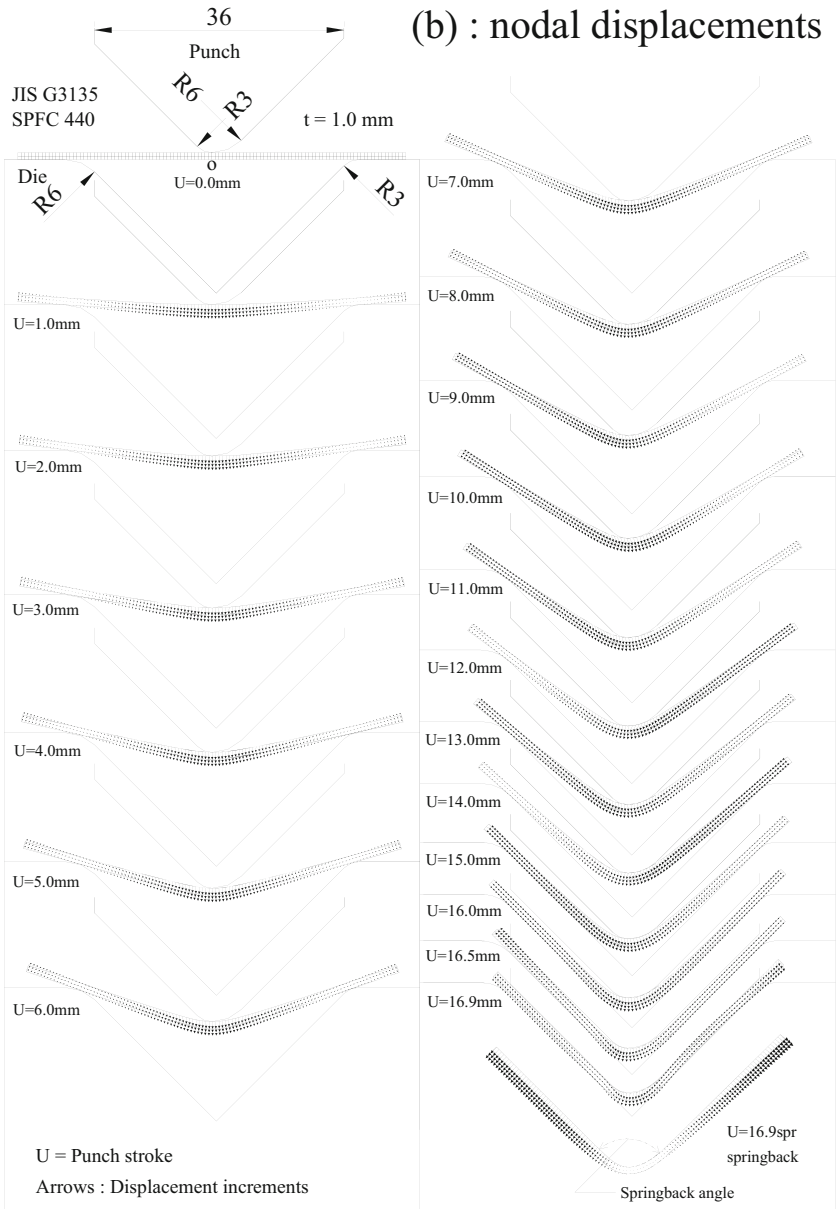

Fig. 4 (continued)

important role of punch radius on deviation change. The opposite effect may result from the increased friction force, which increases the bending moment on the side of small punch and die radii. The deviation change obtained by the punch with Rp1=3 mm and Rp2=6 mm is substantially smaller than that obtained by the punch with Rp1=6 mm and Rp2=3 mm. Regarding die geometry, the sheet moving into the die cavity is restricted by the effect of the small Rd on the small Rp, which induces a large bending moment and a large friction force. Thus, the movement of the sheet from the large Rd side to the small Rd side increases, which increases the bending deviation.

(2) Springback angle (positive value shows springback angle and negative value shows springforward angle): Figs. 10, 11, 12, and 13 show the effects of various process parameters on springback angle. Figure 10 shows that springback occurs when Rp1=6 mm and Rp2=3 mm (punch: R6–R3) and increases as material strength increases under Rd1=6 mm, Rd2=3 mm, W=36 mm, dry friction, and t=1.8 mm. However, springforward (the reverse of springback) occurs when Rp1=3 mm and Rp2=6 mm (punch: R3–R6) and increases as material strength increases under same Rd1, Rd2, W, lubrication, and t. The punch radius substantially affects the alteration between springback and

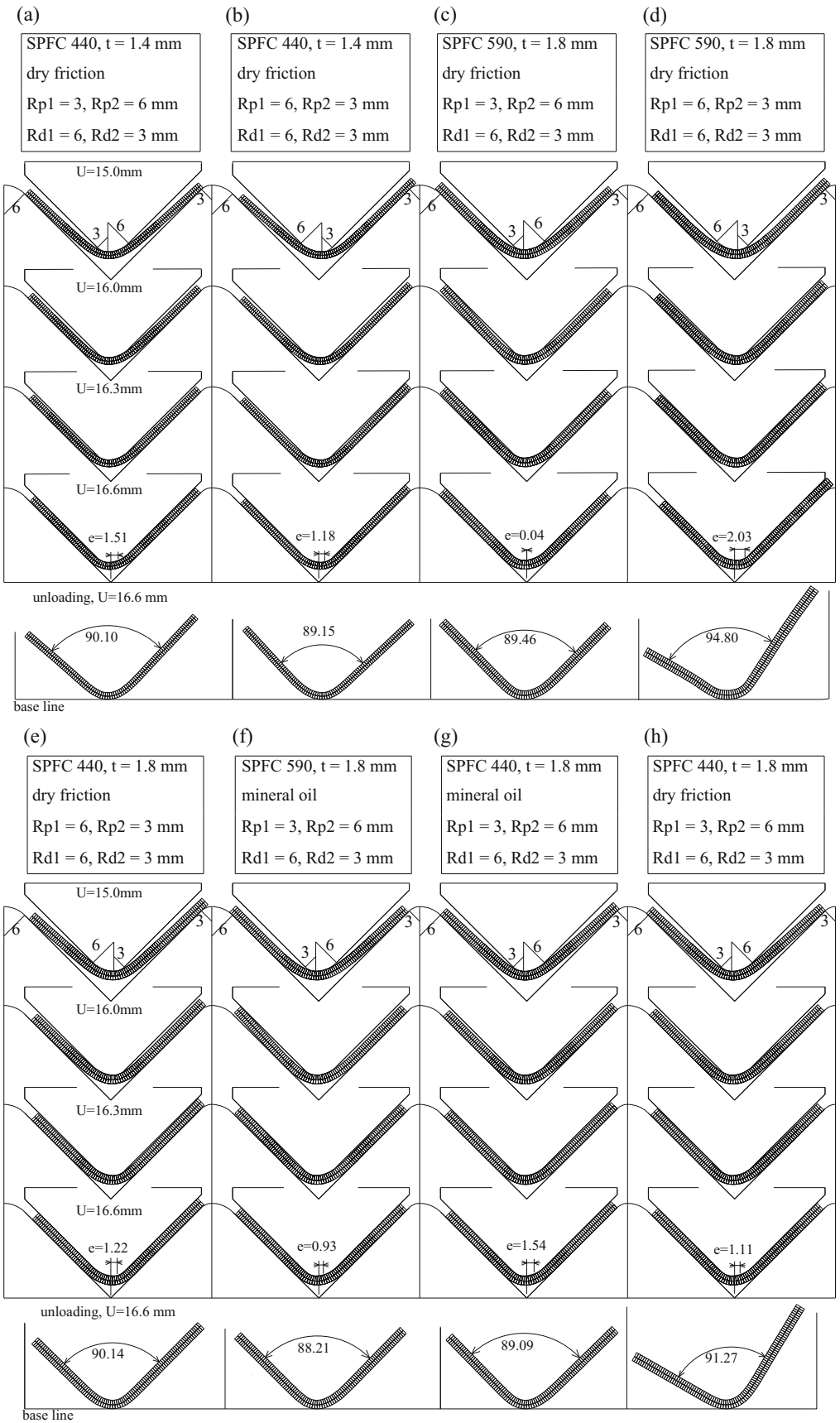

Fig. 5 Deformed shapes for eight process conditions of asymmetric V-die bending shown in Table 2

Table 2 Experimental and calculated values for deviation in asymmetric V-die bending process

Case		1	2	3	4	5	6	7	8
Punch Rp1-Rp2		R6-R3	R6-R3	R6-R3	R3-R6	R3-R6	R3-R6	R3-R6	R3-R6
Die Rd1-Rd2		R6-R3	R6-R3	R6-R3	R6-R3	R6-R3	R6-R3	R6-R3	R6-R3
Thickness		1.8	1.4	1.8	1.4	1.8	1.8	1.8	1.8
Material		590	440	440	440	440	440	590	590
Lubricant		No	No	No	No	Oil	No	Oil	No
Dev	Cr	2.03	1.18	1.22	1.51	1.54	1.11	0.93	0.04
	Er	1.45	0.89	1.13	1.16	1.18	0.85	0.74	0.16
	Err	0.58	0.29	0.09	0.35	0.36	0.26	0.19	−0.12
Spa	Cr	94.8	89.15	90.14	90.10	89.09	91.27	88.21	89.46
	Er	91.0	89.20	90.90	90.55	89.15	89.85	89.20	89.75
	Err	3.80	−0.05	−0.76	−0.45	−0.06	1.42	−0.99	−0.29

Rp1-Rp2 Rp1 is the radius of punch in the left side. Rp2 is the radius of punch in the right side. *Rd1-Rd2* Rd1 is the radius of die in the left side; Rd2 is the radius of die in the right side

Er experimental data, *Cr* calculated value, *Err* error (= Cr–Er), *Dev* deviation, *Spa* springback angle, *Oil* mineral oil WD-40

springforward. This reverse effect may result from the difference in bending moment between the punch contact and the die contact regions, which changes the springback effect to a springforward effect. The larger material strength results in a greater springback or springforward, which may result from an increased elastic strain during unloading as material strength increases. Figure 11 shows that springforward occurred at t= 1.4 mm and springback occurred at t=1.8 mm when parameters were set to Rp1=6 mm and Rp2=3 mm under Rd1=6 mm, Rd2=3 mm, W=36 mm, dry friction, and SPFC 440. Conversely, springforward occurred at t=1.8 mm and springback occurred at t=1.4 mm when parameters were set to Rp1=3 mm and Rp2=6 mm under Rd1=6 mm, Rd2=3 mm, W=36 mm, dry friction, and SPFC 440. Notably, this reverse effect, *i.e.*, the changes from springback to springforward, shows the important roles of thickness and punch radius in elastic recovery and in the direction of unloading, *i.e.* springback or springforward, during unloading. Because of these complicated interacting effects, the unloading characteristics of asymmetric bending are unclear. Figure 12 shows the effect of lubrication on springback for SPFC 440 and 590. Springforward occurs when the

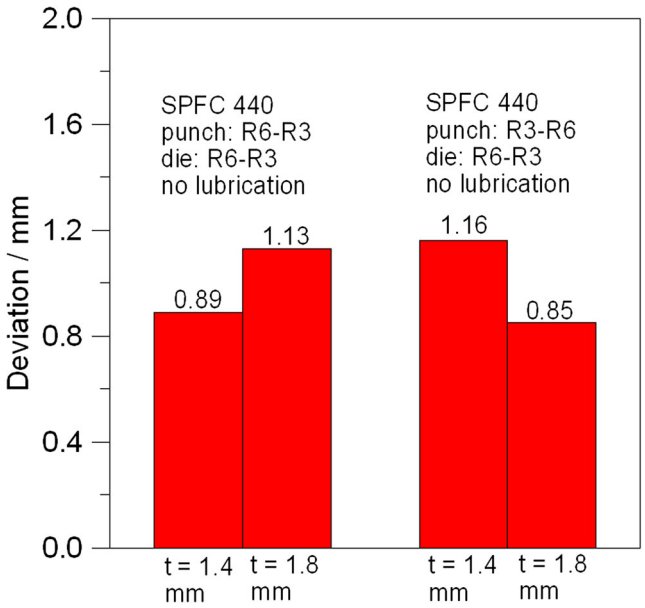

Fig. 6 Experimental values for deviation obtained under varying thickness and punch radius under Rd1=6 mm, Rd2=3 mm, W=36 mm, dry friction, and SPFC 440

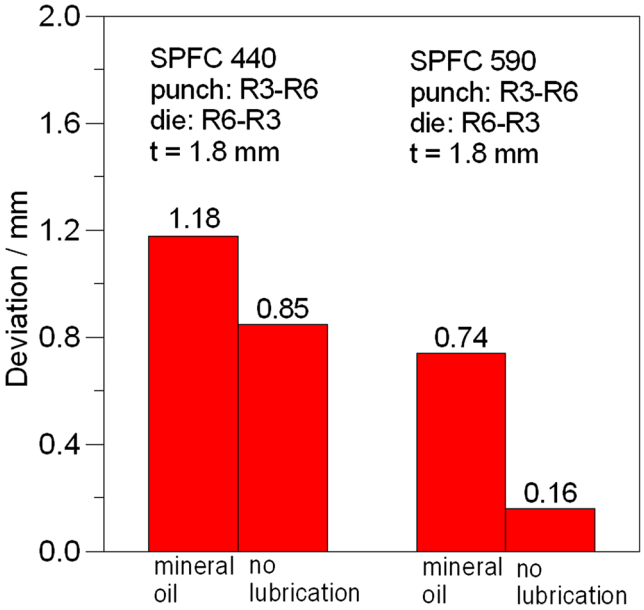

Fig. 7 Experimental values for deviation obtained under varying material strength and lubrication under Rp1=3 mm, Rp2=6 mm, Rd1=6 mm, Rd2=3 mm, W=36 mm, and t=1.8 mm

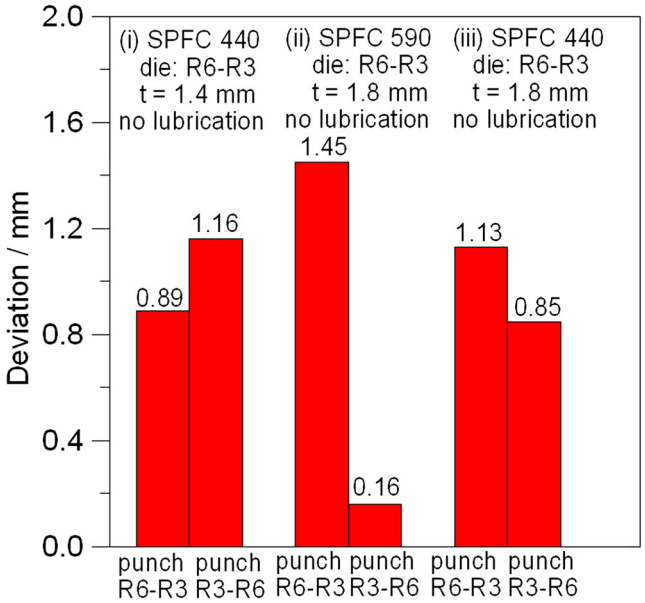

Fig. 8 Experimental values for deviation obtained under varying material strength, punch radius, and thickness under Rd1=6 mm, Rd2=3 mm, W=36 mm, and dry friction

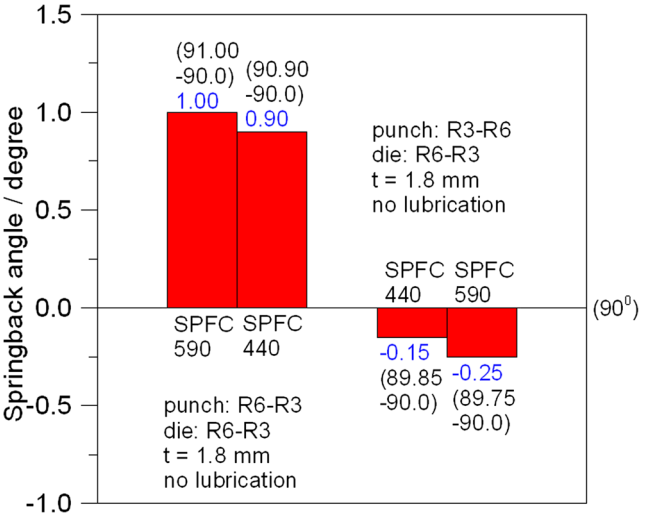

Fig. 10 Experimental values for springback angle obtained for varying material strength and punch radius under Rd1=6 mm, Rd2=3 mm, W=36 mm, t=1.8 mm, and dry friction

parameters are set to Rp1=3 mm, Rp2=6 mm, Rd1=6 mm, Rd2=3 mm, t=1.8 mm, and W=36 mm for SPFC 440 and 590. Accordingly, springforward obtained in the mineral oil WD-40 case is significantly greater than that obtained in the dry friction case for both SPFC 440 and 590. The large difference in springforward angle between dry friction and lubrication confirms the important role of lubrication in elastic recovery. Notably, springforward increases as friction decreases (lubricant added), which may result from the reduced resistance of movement resulting from lubrication in the contact region. In this test, material strength apparently has a limited effect on the alternation between springback and springforward. Cases (ii) and (iii) in Fig. 13 show that springback consistently occurred when Rp1=6 mm and Rp2=3 mm and when other parameters were set to Rd1=6 mm, Rd2=3 mm, t=1.8 mm, W=36 mm and dry friction for both SPFC 440 and 590. Conversely, springforward consistently occurred when Rp1=3 mm and Rp2=6 mm under same Rd1, Rd2, t, W, and lubrication for both SPFC 440 and 590. Punch radius clearly plays an important role in the alternation between springback and springforward. Cases (i) and (iii) in Fig. 13 show that springforward occurred when Rp1=

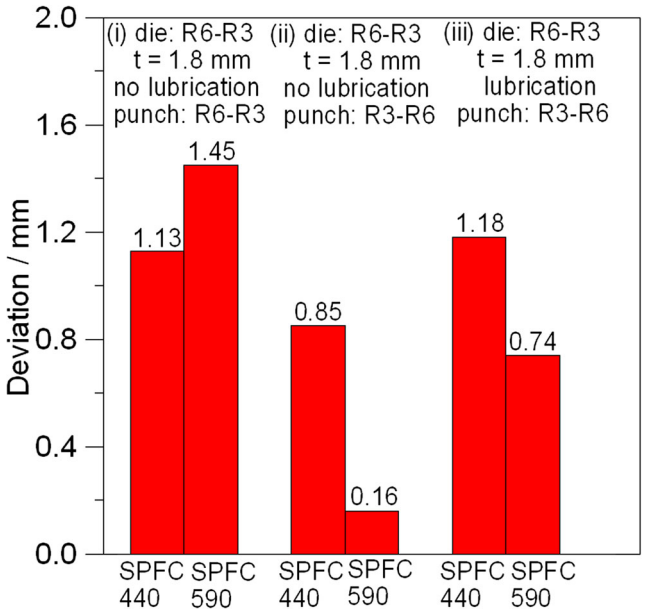

Fig. 9 Experimental values for deviation obtained under varying material strength, punch radius, and lubrication under Rd1=6 mm, Rd2=3 mm, W=36 mm, and t=1.8 mm

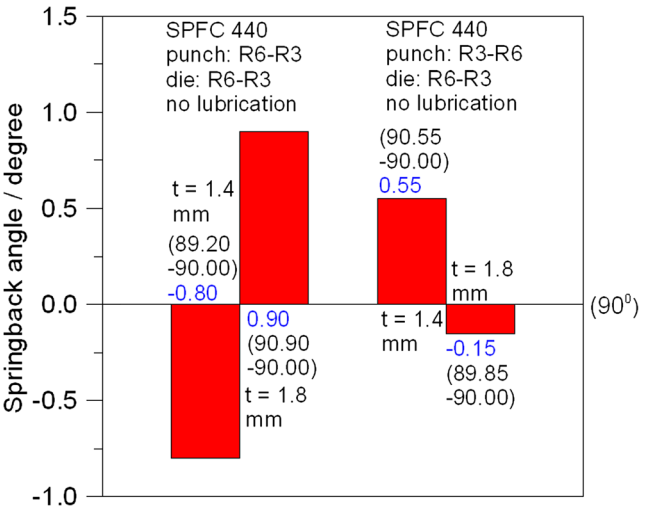

Fig. 11 Experimental values for springback angle obtained under varying thickness and punch radius under Rd1=6 mm, Rd2=3 mm, W=36 mm, dry friction, and SPFC 440

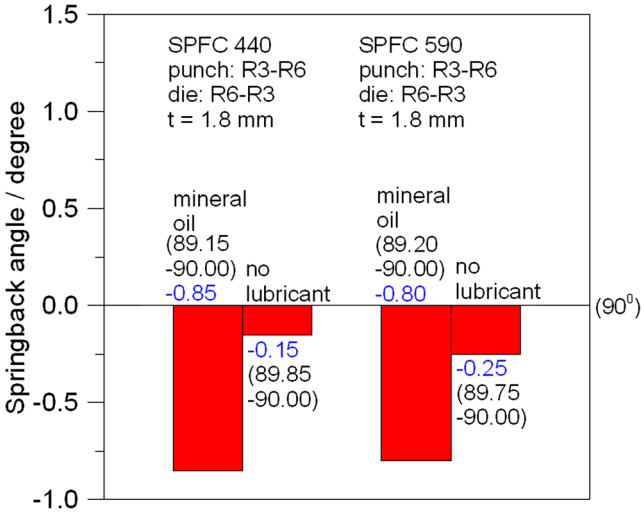

Fig. 12 Experimental values for springback angle obtained under varying lubrication and material strength under Rp1=3 mm, Rp2=6 mm, Rd1=6 mm, Rd2=3 mm, W=36 mm, and t=1.8 mm

6 mm and Rp2=3 mm, and springback occurred when Rp1=3 mm and Rp2=6 mm under parameter settings of Rd1=6 mm, Rd2=3 mm, W=36 mm, dry friction, t=1.4 mm, and SPFC 440 in case (i). Conversely, springforward occurred when Rp1=3 mm, Rp2=6 mm, and springback occurred when Rp1=6 mm, Rp2=3 mm under parameter settings of Rd1=6 mm, Rd2=3 mm, W=36 mm, dry friction, t=1.8 mm, and SPFC 440 in case (iii). Notably, t=1.4 mm, Rp1=3 mm, and Rp2=6 mm induce springback; however, t=1.8 mm, Rp1=3 mm, and Rp2=6 mm induce springforward when all other conditions are similar. Conversely, the reverse effect is obtained when t=1.4 mm, Rp1=6 mm and Rp2=3 mm, which induces springforward; whereas, t=1.8 mm, Rp1=6 mm, and Rp2=3 mm induce springback. The reverse results clearly show the important roles of thickness and punch radius in elastic recovery after unloading of bending. During this complex interaction, thickness apparently counteracts the punch radius effect on the change of the alternate springback and springforward.

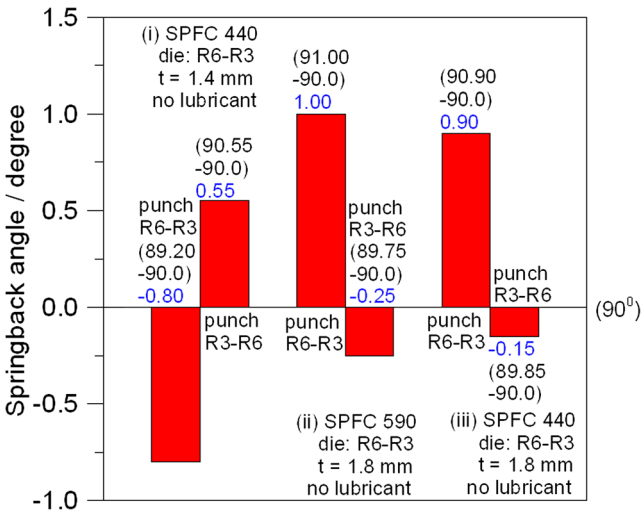

Fig. 13 Experimental values for springback angle obtained under varying punch radius, thickness, and material strength under Rd1=6 mm, Rd2=3 mm, W=36 mm, and dry friction

The analysis shows that the interaction of process parameters is very complex and irregular. The process parameters cannot be considered in isolation. Therefore, further studies are needed to elucidate complex interactions among process parameters.

4 Conclusions

This pioneering work in the use of asymmetric tools to analyze asymmetric V-die bending process yielded the following findings.

1. Deviation: The effect of process parameters on position deviation is varied and complex. (1) Increased sheet thickness, high material strength and high friction (without lubrication) generally reduce deviation under the conditions of Rp1=3 mm and Rp2=6 mm. Moreover, the effect of thickness on deviation is larger than the effect of punch radius. (2) Conversely, a small sheet thickness apparently reduces deviation under the conditions of Rp1=6 mm and Rp2=3 mm. A high material strength also effectively increases deviation. (3) In conclusion, the effect of sheet thickness apparently counteracts the effect of punch radius on deviation change under certain conditions, and this interaction is very complex.
2. Elastic recovery (springback or springforward): The effect of process parameters on elastic recovery is varied and complex. (1) Generally, a large sheet thickness, high material strength and low friction (lubricant added) effectively increase the occurrence of springforward under the conditions of Rp1=3 mm and Rp2=6 mm. However, the occurrence of springback (the reverse of springforward) increases as Rp1=3 mm and Rp2=6 mm used for a small sheet thickness. In terms of elastic recovery, sheet thickness is apparently more important than punch radius. (2) Conversely, a small sheet thickness apparently increases the occurrence of springforward under the conditions of Rp1=6 mm and Rp2=3 mm. Under similar conditions, a large sheet thickness increases the occurrence of springback. (3) In conclusion, the effect of sheet thickness apparently counteracts the effect of punch radius on springback under certain conditions. Therefore, sheet thickness apparently has an important role in springback formation.

3. Finite element simulations of deviation and elastic recovery agreed well with the experimental results in this work. The FE simulations show the region of plastic deformation, which indicates the overall process of deformation. They also show the material flow during incremental changes in the distribution of displacement, which indicates position deviation based on movement of the bending point. Accordingly, a springback or springforward phenomenon can be simulated to show the final shape of the component after all tools are removed for elastic unloading. In conclusion, the effects of process parameters such as sheet thickness, punch radius, material strength and lubrication, on springback and on deviation vary. Therefore, this study indicates that the interaction of process parameters is very complicated and irregular. The process parameters cannot be considered in isolation. Finite element simulation is a powerful tool for simulating the complex interacting effects of process parameters when designing an asymmetric bent component without bending deviation.

Acknowledgments The author would like to thank the National Science Council of the Republic of China, Taiwan for financially supporting this research under Contract No. NSC 102-2221-E-149-001. Ted Knoy is appreciated for his editorial assistance, and C. L. Yang, Y. C. Lee, and Z. C. Chen are appreciated for helpful discussions.

References

1. Gardiner FJ (1957) The springback of metals. ASME J Appl Mech 79:1–9
2. Weinmann KJ, Shippell RJ (1978) Effect of tool and workpiece geometries upon bending forces and springback in 90 degree V-die bending of HSLA steel plate. Proceeding of the Sixth North American Metal Working Research Conference, pp 220–227
3. Huang YM, Takizawa H, Makinouchi A, Nakagawa T (1989) Elastic–plastic analysis of V-bending process. Spring Proc. Plastic Working, Cho-Fu, Tokyo, pp 275–278
4. Huang YM, Lu YH, Makinouchi A (1992) Elasto-plastic finite-element analysis of V-shape sheet bending. J Mater Process Technol 35:129–150
5. Ogawa H, Makinouchi A, Takizawa H, Mori N (1993) Development of an elasto-plastic FE code for accurate prediction of springback in sheet bending processes and its validation by experiments. Advanced Technology of Plasticity, Proceeding of the Fourth International Conference on Technology of Plasticity, pp 1641–1646
6. Huang YM, Chen TC (2005) Influence of blank profile on the V-die bending camber process of sheet metal. Int J Adv Manuf Technol 25: 668–677
7. Huang YM (2007) Finite element analysis on the V-die coining bend process of steel metal. Int J Adv Manuf Technol 34:287–294
8. Thipprakmas S (2013) Finite element analysis of sided coined-bead technique in precision V-bending process. Int J Adv Manuf Technol 65:679–688
9. Datsko J, Yang CT (1960) Correlation of bendability of materials with their tensile properties. ASME J Eng Ind :309–314
10. Takenaka N, Tozawa Y, Suzuki K (1971) Material characteristic value for evaluation of bendability and methods for measuring these values. Ann CIRP 20:53–54
11. Cupka V, Nakagawa T, Tiyamoto H, Kudo H (1973) Fine bending with counter pressure. Ann CIRP 22:73–74
12. Kals JAG, Veenstra PC (1974) On the critical radius in sheet bending. Ann CIRP 23:55–56
13. Wang C, Kinzel G, Altan T (1993) Mathematical modeling of plane-strain bending of sheet and plate. J Mater Process Technol 39:279–304
14. Leu DK (1997) A simplified approach for evaluation bendability and springback in plastic bending of anisotropic sheet metals. J Mater Process Technol 66:9–17
15. Bakhshi-Jooybari M, Rahmani B, Daeezadeh V, Gorji A (2009) The study of spring-back of CK67 steel sheet in V-die and U-die bending processes. Mater Des 30(7):2410–2419
16. Narayanasamy R, Padmanabhan P (2009) Application of response surface methodology for predicting bend force during air bending process in interstitial free steel sheet. Int J Adv Manuf Technol 44: 38–48
17. Farsi MA, Arezoo B (2009) Development of a new method to determine bending sequence in progressive dies. Int J Adv Manuf Technol 43:52–60
18. Yu HY (2009) Variation of elastic modulus during plastic deformation and its influence on springback. Mater Des 30: 846–850
19. Ramezani M, Mohd Ripin Z, Ahmad R (2010) Modelling of kinetic friction in V-bending of ultra-high-strength steel sheets. Int J Adv Manuf Technol 46:101–110
20. Ramezani M, Mohd Ripin Z (2010) A friction model for dry contacts during metal-forming processes. Int J Adv Manuf Technol 51:93–102
21. Kardes Sever N, Mete OH, Demiralp Y, Choi C, Altan T (2012) Springback prediction in bending of AHSS-DP 780. Proc NAMRI/SME 40:1–10
22. Fu ZM (2012) Numerical simulation of springback in air-bending forming of sheet metal. Appl Mech Mater 121–126:3602–3606
23. Fu Z, Mo J (2011) Springback prediction of high-strength sheet metal under air bending forming and tool design based on GA–BPNN. Int J Adv Manuf Technol 53(5–8):473–483
24. Malikov V, Ossenbrink R, Viehweger B, Michailov V (2012) Experimental investigation and analytical calculation of the bending force for air bending of structured sheet metals. Adv Mater Res 418–420:1294–1300
25. Duc-Toan N, Seung-Han Y, Dong-Won J, Tien-Long B, Young-Suk K (2012) A study on material modeling to predict spring-back in V-bending of AZ31 magnesium alloy sheet at various temperatures. Int J Adv Manuf Technol 62:551–562
26. Leu DK (2013) Position deviation in V-die bending process with asymmetric bend length. Int J Adv Manuf Technol 64:93–103
27. McMeeking RM, Rice JR (1975) Finite element formulations for problems of large elastic–plastic deformation. Int J Solids Struct 11: 601–606
28. Oden JT, Pries EB (1983) Nonlocal and nonlinear friction law and variational principles for contact problems in elasticity. ASME J Appl Mech 50:67–76
29. Yamada Y, Yoshimura N, Sakurai T (1968) Plastic stress–strain matrix and its application for the solution of elastic–plastic problems by the finite element method. Int J Mech Sci 10: 343–354
30. Leu DK (1996) Finite-element simulation of hole-flanging process of circular sheets of anisotropic materials. Int J Mech Sci 38(8–9):917–933
31. Leu DK (1998) Effects of process variables on V-die bending process of steel sheet. Int J Mech Sci 40(7):631–650